RSC Advances

ROYAL SOCIETY OF CHEMISTRY

www.rsc.org/advances

Graphic Abstract

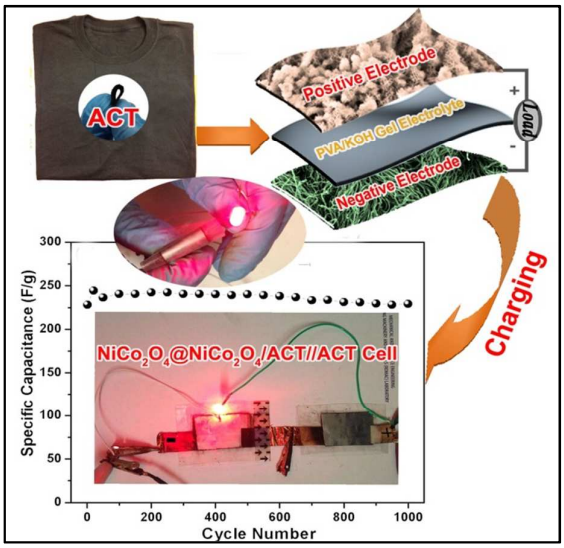

Table of Content

Hierarchical $NiCo_2O_4$@$NiCo_2O_4$ core/shell nanostructure was grown on flexible, cotton activated carbon textiles (ACTs) to fabricate $NiCo_2O_4$@$NiCo_2O_4$/ACT electrodes. The assembled flexible $NiCo_2O_4$@$NiCo_2O_4$/ACT//ACT asymmetric exhibited an exceptional combination of electrochemical and mechanical properties.

RSC Advances

RSC Publishing

ARTICLE

Cotton Textile Enabled, All-Solid-State Flexible Supercapacitors

Zan Gao,[a] Ningning Song,[a] Yunya Zhang, [a] and Xiaodong Li*[,a]

Cite this: DOI: 10.1039/x0xx00000x

Received 00th XX 2015,
Accepted 00th XX 2015

DOI: 10.1039/x0xx00000x

www.rsc.org/

Hierarchical $NiCo_2O_4$@$NiCo_2O_4$ core/shell nanostructure was grown on flexible cotton activated carbon textiles (ACTs) to fabricate $NiCo_2O_4$@$NiCo_2O_4$/ACT electrodes. After dipped with PVA-KOH polymer gel which served as both the solid state electrolyte and separator, the flexible $NiCo_2O_4$@$NiCo_2O_4$/ACT hybrid electrode exhibited an exceptional combination of electrochemical and mechanical properties in terms of specific capacitance (1929 F/g，based on the mass of $NiCo_2O_4$), energy density (83.6 Wh/kg), power density (8.4 KW/kg), cycling stability, and mechancal roubstness (the tensile strengh is 6.4 times higher than that of pure ACT). The outstanding electrochemical performance is ascribed to the unique core/shell nanostructure with high active-surface area, morphological stability, and short ion transport path. Such hierarchical core/shell nanostructure of the same material on cotton-enabled flexible substrate should inspire us to develop flexible solid-state textile energy storage devices for future wearable electronics.

1. Introduction

In modern society, energy is the lifeblood. To solve the issues of global warming, environment pollution, and the depletion of fossil-fuel, a worldwide imperative is to make the use of sustainable and renewable energy. Numerous energy storage solutions, for instance, mechanical, magnetic and chemical storage, are being intensively investigated to harvest renewable energies, such as solar, wind, geothermal and tidal energy.[1] Batteries, fuel cells, and electrochemical capacitors that can convert chemical energy directly into electrical energy are the most effective technologies for practical electrochemical energy storage and conversion. Recently, supercapacitors (also known as ultracapacitors or electrochemical capacitors) have been regarded as one of the most promising energy storage devices due to their high power performance, long lifespan, and low maintenance cost.[2] Most importantly, supercapacitors fill the power/energy gap between the traditional capacitors (with higher power density) and batteries/fuel cells (with higher energy density),[3] and have shown a great potential in transportation, electrical power, electronics and aviation. Much effort has been devoted to developing lightweight, flexible, and highly efficient power devices to meet the urgent need of flexible/wearable electronics, such as flexible cell phones, roll-up and bendable displays, photovoltaic cells, artificial electronics skin, and distributed sensors.[4]

However, previous research was mainly focused on aqueous solution, organic solution or ionic liquids, which usually brought serious package and safety problem.[5-8] The possible leakage of highly toxic or corrosive electrolyte impedes its practical application in portable/wearable electronics.[9] Solid-state supercapacitors, because of their combined advantages, such as small size, ease of handling, robust mechanical performance, excellent reliability and safety, wide operation temperature range and extended working potential, have attracted more and more attention.[4] Flexible solid-state supercapacitors usually consist of flexible electrodes, solid-state electrolyte, flexible separator and packaging material. As the most crucial functional blocks, flexible electrodes have attracted considerable attention. For instance, carbon materials, such as carbon nanotubes (CNTs), carbon cloth, graphene papers, and carbon fibers, have been intensively investigated as the flexible electrodes duo to their higher power density, longer life cycle, outstanding mechanical robustness and excellent electrical conductivity.[10-14] However, the use of expensive CNTs or graphene to construct flexible electrodes will increase the cost of the device. Another drawback of using CNTs or graphene is their relative low energy density. These two factors more or less hinder its widespread commercialization.

It is imperative to develop wearable energy storage systems for future flexible electronics. To date, however, textile based energy devices are still lacking. Streamlined manufacturing processes for integrating flexible energy storage devices with wearable electronics have not been truly realized.[15] Cotton textiles are the most widely used natural fibers for soft and breathable clothing. In our previous work, we have successfully converted a commercial cotton T-shirt into activated carbon textiles (ACTs) with highly conductivity and flexibility for flexible energy storage application.[16] By integrating ACTs with MnO_2, the textile-based flexible supercapacitors exhibited remarkably enhanced electrochemical performance. To further improve the electrochemical performance of carbon based supercapacitors, pesudocapacitive materials (MnO_2,[17,18] $NiCo_2O_4$,[19] Co_3O_4,[20] NiO[21], LDH[22] and conducting polymer[23,24]) have been used to decorate the surfaces of carbon materials. However, due to the poor conductivity and short ion diffusion path of pseudo-capacitive materials, the electrochemical

[*] Prof. X.D. Li, Z. Gao, N.N. Song, Y.Y. Zhang

Department of Mechanical and Aerospace Engineering
University of Virginia
122 Engineer's Way, Charlottesville, VA 22904-4746 (USA)
E-mail: xl3p@virginia.edu

reaction process happens only on the very surface layer of the electrode, which limits the contribution of the inner active materials to the total capacitance.[25] To make full utilization of pesudocapacitive materials, an intelligent strategy is to compound two types of materials or nanostructures on one conductive substrate with integrated hierarchical architectures, which fully exploit the potential of individual materials and bring together many competitive advantages, such as rich electroactive sites, easy accessibility of electrolyte ions, short diffusion path, superior current collection efficiency and the fascinating synergetic effect of different components.[26-29] For example, Guan *et al*.[30] reported enhanced electrochemical performance (areal capacitance of 2.04 F/cm^2 at the scan rate of 5 mV/s) from hierarchical Co_3O_4@$NiCo_2O_4$ nanoforest on Ni-foam. Daoping *et al*.[31] achieved a specific capacitance of 14.67 F/cm^2 from $NiCo_2O_4$@$CoMoO_4$ core/shell nanowire arrays. Yu *et al.*[32] demonstrated that $NiCo_2O_4$@MnO_2 core/shell pseudocapacitors achieved a specific capacitance of 1.66 F/cm^2. Recently we fabricated Zn_2SnO_4/MnO_2 core/shell nanocables on carbon microfibers and $NiCo_2O_4$@NiO core/shell nanostructure on carbon cloth for high performance flexible electrodes.[33,34] The drawback of the aforementioned core/shell structure is the high contact resistance between the core and shell which are dissimilar materials. It remains a great challenge to synthesize core/shell nanostructures of the same material due to the difficulties in controlling the assembly and fusion of the core and the shell with pre-designed morphologies.[35]

Recently, ternary nickel cobaltite ($NiCo_2O_4$) has been intensively studied as a high-performance electrode material for supercapacitors due to the exceptional combination of its high electrical conductivity and electrochemical activity. Several types of $NiCo_2O_4$ nanostructures including 1D nanowire,[36] 2D nanosheet[37] and 3D urchin-like microsphere[38] have shown great promise for supercapacitor applications. Although the capacitive performance of various nanostructures has been intensively investigated, there are rarely reports about the integration of hierarchical nanostructures comprised of the same material with different morphologies.

In this study, we synthesized hierarchical $NiCo_2O_4$@$NiCo_2O_4$ core/shell nanostructure on highly flexible and conductive activated carbon textiles (ACTs) which were converted directly from cotton textiles. The conductive $NiCo_2O_4$ nanowires, radially anchored on the ACT fibers, served as cores (backbones) to support the $NiCo_2O_4$ nanoflake shells to form a hierarchical 3D porous nanostructure of the same material. Such scaffold-like porous architecture served as a reservoir for electrolyte ions, providing highly electrolytic accessible surface area, robust electrical connection to substrate and short ion diffusion path. The nanowire core and nanoflake shell are of the same material, thereby eliminating the contact resistance between the core and the shell, enabling a fast reversible Faradaic reaction and full utilization of active materials during charge-discharge process. After dipped in polyvinyl alcohol (PVA)/KOH solid-state electrolyte, the interspace of the $NiCo_2O_4$@$NiCo_2O_4$ core/shell scaffold-like architecture was completely filled with gel electrolyte which concurrently served as separator, not only improving the accessibility of electrolyte ions but also intensifying the mechanical strength of the flexible electrode. The fabricated flexible $NiCo_2O_4$@$NiCo_2O_4$/ACT hybrid electrode achived an exceptional combination of electrochemcial and mechanical properties in terms of specific capacitance (1929 F/g), energy density (83.6 Wh/kg), power density (8.4 KW/kg), cycling stability, and mechancal roubstness (the tensile strengh is 6.4 times higher than that of pure ACT). Such hierarchical core/shell nanostructure of the same material on cotton-enabled flexible substrate should inspire us to develop flexible solid-state textile energy storage devices for future wearable electronics.

2. Experimental Section

2.1 Preparation of Flexible $NiCo_2O_4$@$NiCo_2O_4$/ACT Electrode

Activation of cotton textile

All the chemicals were of analytical grade (purchased from Sigma) and used without further purification. A commercial cotton T-shirt was cleaned in distilled water prior to activation. Activation of cotton T-shirt textile was performed following our previous report.[16] Briefly, a piece of pure cotton T-shirt was firstly dipped into 1 M NaF solution and kept for 1 h. The dipped textile was then dried at 120 ℃ for 3 h. Finally, the dried, NaF-treated cotton textile was inserted into a horizontal tube furnace and heated at 1000 ℃ for 1 h with a continuous argon gas flow. After cooling down to room temperature, the as-obtained activated cotton textiles were washed with distilled water to remove the residual NaF, and then dried at 80 ℃ for 6 h.

Fabrication of $NiCo_2O_4$ nanowires on activated cotton textiles

$NiCo_2O_4$ nanowires were radically grown on the ACT fibers via a simple hydrothermal process. Typically, 1.45 g of $Ni(NO_3)_2{\cdot}6H_2O$, 2.91 g of $Co(NO_3)_2{\cdot}6H_2O$, and 0.9 g of urea were dissolved in 70 mL of distilled water to form a pink-color solution. Then, the solution was transferred into a 100 mL Teflon-lined stainless autoclave with a piece of ACT (1 cm × 2 cm) vertically suspended in the solution. After that, the autoclave was kept at 120 ℃ in an electric oven for 12 h. Finally, the as-synthesized products were taken out, washed with ethanol and distilled water for several times, dried at 80 ℃ overnight, and annealed at 400 °C in argon atmosphere for 2 h to produce $NiCo_2O_4$ nanowire/ACT. The mass loading of $NiCo_2O_4$ nanowires on activated carbon textiles was measured to be 2.12 mg/cm^2.

Coating $NiCo_2O_4$ nanoflakes onto $NiCo_2O_4$ nanowires

The shell layer of $NiCo_2O_4$ nanoflakes was prepared by a simple chemical bath deposition process.[39] Typically, 2 mL of aqueous ammonia (25-28%) was added to the mixture of 5 mL of 1 M nickel sulfate, 5 mL of 2 M cobalt nitrate, and 8 mL of 0.25 M potassium persulfate to form chemical bath deposition solution. After that, the obtained $NiCo_2O_4$ nanowire/ACT was vertically placed in the fresh, chemical bath deposition solution and kept for 10 min at room temperature for coating the Ni-Co hydroxide precursor shell. After the deposition, the sample was rinsed with distilled water and then dried at 80 °C for 12 h in an electric oven. Finally, the obtained hybrid was further annealed at 400 ℃ under argon protection for 2 h to obtain the flexible $NiCo_2O_4$@$NiCo_2O_4$/ACT electrode. The mass loading of $NiCo_2O_4$@$NiCo_2O_4$ on activated carbon textiles was measured to be 2.63 mg/cm^2.

2.2 Characterization Methods

The crystallographic structure of the synthesized materials were determined by a PANalytical X'Pert Pro Multi-Purpose Diffractometer (MPD) equipped with Cu K_α radiation (λ = 0.15406 nm). The microstructure of the samples was characterized by scanning electron microscopy (SEM; FEI Quanta 650) and transmission electron microscopy (TEM; Philips CM 200 FEG, 160 kV). X-ray photoelectron spectroscopy (XPS) measurements were performed using a PHI 5700 ESCA spectrometer with monochromated Al KR radiation (hv = 1486.6 eV). All the XPS spectra were corrected by the C1s line at 284.5 eV.

2.3 Fabrication and Electrochemical Characterization of Flexible All-Solid-State Supercapacitors

The flexible supercapacitors were assembled with two pieces of flexible electrodes (2 cm × 1 cm) face-to-face separated by the solid-state polymer electrolyte. The PVA/KOH gel was prepared by mixing 3 g KOH and 6 g PVA in 60 mL deionized water and heated to 80 ºC under stirring until the solution became clear. A flat Petridish was used to prepare a thin KOH/PVA film by a natural solidification process. Prior to assembly, the fabricated flexible electrodes were first dipped into the gel electrolyte for 3 min to ensure that the internal interspace of active materials was completely filled with the electrolyte. After solidified at room temperature, the solid-state flexible supercapacitor was fabricated with a KOH/PVA film by mechanical pressing. The KOH/PVA film served as both the separator and electrolyte.

The electrochemical characterization was carried out using a CHI 660E electrochemical workstation. The comprehensive lectrochemical properties of the as-obtained products and assembled flexible supercapacitors were investigated by both three-electrode and two-electrode electrochemical systems. For the three-electrode system, ACT, $NiCo_2O_4$ nanowire/ACT and $NiCo_2O_4$@$NiCo_2O_4$/ACT electrodes were directly used as the working electrode, a platinum foil (1 cm × 1 cm) and a saturated calomel electrode (SCE) were used as the counter and reference electrodes, respectively. The three-electrode tests were carried out in 6 M KOH aqueous electrolyte at room temperature. Cyclic voltammograms (CV), galvanostatic charge/discharge curves, and electrochemical impedance spectroscopy (EIS) in the frequency range from 100 kHz to 0.05 Hz with an AC perturbation of 5 mV were used to evaluate the electrochemical performance of the flexible electrode. Asymmetric and symmetric flexible cells were also assembled by using ACT, $NiCo_2O_4$ nanowire/ACT and $NiCo_2O_4$@$NiCo_2O_4$/ACT as the flexible electrodes, conductive copper tape attached on the PET film as current collectors, and the as-made solid-state polymer PVA/KOH gel film severed as both the separator and electrolyte sandwiched between the two electrodes. The total electrode masses (including ACT) are 11.12 mg and 10.71 mg for the symmetric and asymmetric supercapacitors, respectively.

3. Results and Discussion

3.1 Structural and Morphological Characterization

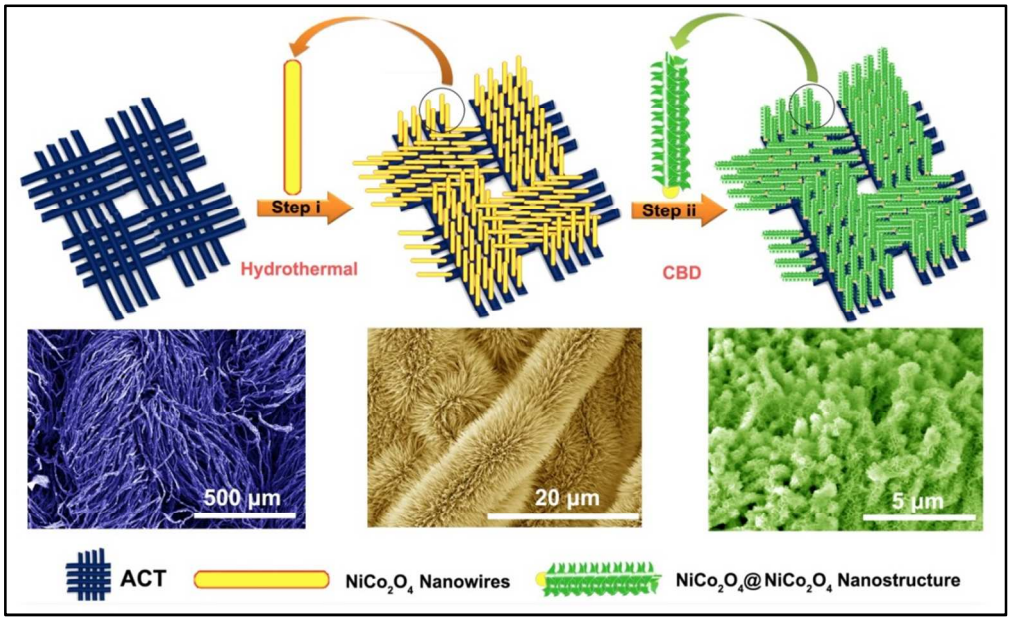

Fig. 1 Illustration of the fabrication process of hierarchical $NiCo_2O_4$@$NiCo_2O_4$ core/shell nanostructure on activated carbon textiles (ACTs).

Fig. 1 shows the design wisdom and fabrication procedure of hierarchical $NiCo_2O_4$@$NiCo_2O_4$ core/shell nanostructure on ACTs. In a typical experiment, $NiCo_2O_4$ nanowire arrays were first radially grown on ACT fibers using a facile hydrothermal method, followed by a calcination process under argon protection (Step i). The hydrothermally synthesized $NiCo_2O_4$ nanowire arrays then served as the backbone for the deposition of $NiCo_2O_4$ nanoflakes by a chemical bath deposition method (Step ii). Such a hierarchical nanostructure ($NiCo_2O_4$ nanowire core/$NiCo_2O_4$ nanoflake shell) on conductive ACTs provides plenty of interspaces, which not only increase electrolyte ion accessibility but also short the transport path, jointly improving the electrochemical performance.

The highly conductive and flexible ACTs were fabricated by direct conversion of a commercial cotton T-shirt through a dipping, drying and curing process as described in our previous report. Fig. 2a shows the digital photograph of a commercial cotton T-shirt, which was used to prepare ACTs. Fig. 2b shows

the digital photograph of a piece of ACT, which is mechanically flexible even under folding state (Fig. 2c) and highly conductive (resistance ~10-20 Ω sq^{-1}). SEM image of

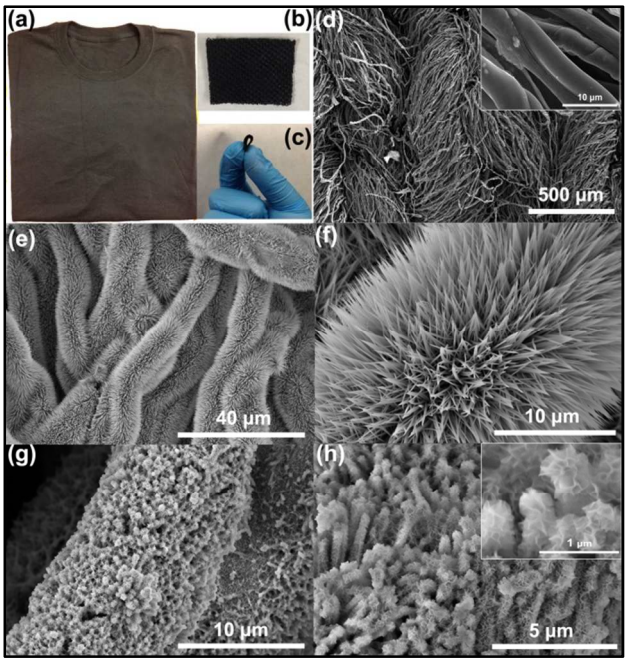

Fig. 2 Optical photographs of (a) a commercial cotton T-shirt, (b) a piece of ACT and (c) a piece of ACT under folding condition, showing its super flexibility; (d) SEM image of ACT, inset is the amplified SEM image; (e-f) SEM images of $NiCo_2O_4$ nanowires grown on the ACT microfibers by a hydrothermal method; (g) and (h) SEM images of $NiCo_2O_4$@$NiCo_2O_4$ core/shell nanostructure on the ACT fibers, inset is the SEM image of $NiCo_2O_4$@$NiCo_2O_4$ nanoflake at high magnification.

ACT shows that the interwoven fibers of activated textile have the diameters ranging from 5 to 10 μ m, which inherit the cellulose fiber architecture of cotton textile (Fig. 2d). Fig. 2e-f shows the morphology of $NiCo_2O_4$ nanowires hydrothermally grown on the surface of ACT. High-density of $NiCo_2O_4$ nanowires, with the length of several micrometers and diameter of around 70 nm, were radially aligned on individual ACT fibers, forming uniform nano-arrays with highly open and porous structure. After the coupled chemical bath deposition and following-up heat treatment, the surfaces of individual $NiCo_2O_4$ nanowires were uniformly decorated with $NiCo_2O_4$ nanoflakes (Fig. 2g-h). The cross-sectional and side-view images of the $NiCo_2O_4$@$NiCo_2O_4$ core/shell nanoarchitecture (Figure 2g and k) jointly reveal that the tiny flaky $NiCo_2O_4$ nanosheets (< 10 nm) were densely anchored on individual $NiCo_2O_4$ nanowires. Of importance, the nanowire core and nanoflake shell are of the same material $NiCo_2O_4$, thereby eliminating the contact resistance between the core and shell and ultimately enhancing both energy and power densities. The tiny $NiCo_2O_4$ nanoflakes render a highly porous hierarchical architecture, which serves as a reservoir for electrolyte ions, providing dense diffusion channels for energy storage.

The chemical compositions of the $NiCo_2O_4$ nanowire/ACT were further analyzed by energy-dispersive X-ray spectrometry (EDS) (Fig. S1 in the Supporting Information). The Ni/Co atomic ratio is 10:19, which is close to the theoretical atomic ratio (1:2) of $NiCo_2O_4$, indicating that the Ni-Co hydroxide precursors were entirely transformed into the $NiCo_2O_4$ after the heat treatment, which agrees well with the XRD result (Fig. 4b), conforming the ACT microfibers were uniformly covered by the $NiCo_2O_4$ nanowire arrays.

The structure and morphology of Ni-Co hydroxide precursors, $NiCo_2O_4$ nanowire/ACT and $NiCo_2O_4$@$NiCo_2O_4$/ACT hybrids were further investigated by TEM. As illustrated in Fig. 3a, the Ni-Co hydroxide precursor nanowires have smooth surface with a diameter of about 50 nm and plenty of mesopores with the size of 2-4 nm inside individual $NiCo_2O_4$ nanowires (Fig. 3b). Such internal active surface areas further enhance the pseudocapacitance. The mesoporous $NiCo_2O_4$ nanowires are anticipated to exhibit unusually high electrochemical properties because of the high density of active sites and short electron transport path.[40] Clearly, such $NiCo_2O_4$ nanowires provide a unique backbone for the design of hierarchal nanoarchitecture with the goal to further push up the electrochemical properties. After the chemical bath deposition, the $NiCo_2O_4$ nanowires were elegantly wrapped with leaf-like $NiCo_2O_4$ nanoflakes, forming a core/shell hierarchical nanoarchitecture of the same material-$NiCo_2O_4$, with high porosity (Figs. 3c-d). Figs. 3e and f show

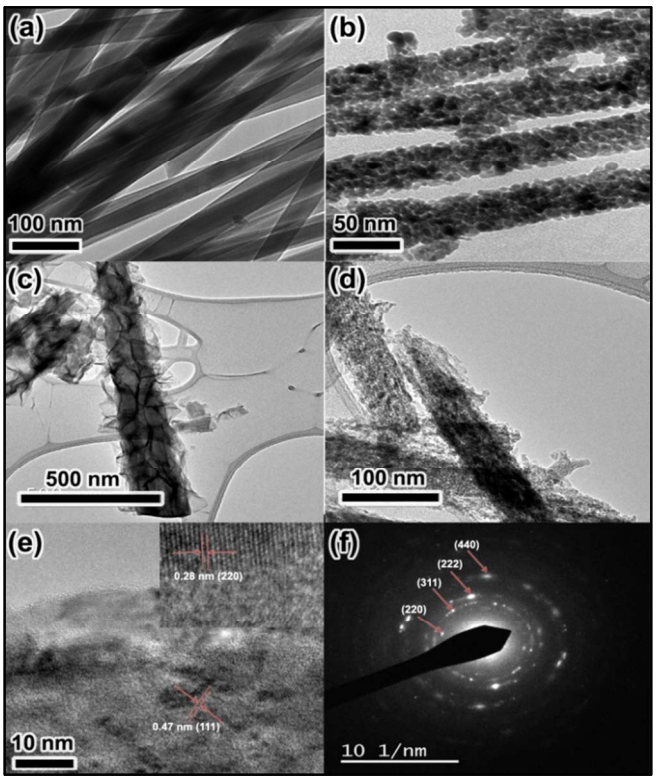

Fig. 3 (a) TEM image of Ni-Co hydroxide precursor naonwires; (b) TEM image of $NiCo_2O_4$ nanowires grown on ACTs after the annealing process; (c) TEM image of $NiCo_2O_4$@$NiCo_2O_4$ core/shell nanostructure precursor; (d) TEM image of $NiCo_2O_4$@$NiCo_2O_4$ core/shell nanostructure after the annealing process; (e) HRTEM image of $NiCo_2O_4$@$NiCo_2O_4$ nanostructure, inset is the amplified region; (f) Selected area electron diffraction (SAED) pattern of $NiCo_2O_4$@$NiCo_2O_4$ nanostructure.

the HRTEM image and SAED pattern of $NiCo_2O_4$@$NiCo_2O_4$ nanostructure. A grain boundary was observed between the core and shell, with the d-spacing of 0.47 nm for the core and 0.28 nm for the shell, indicating different growth direction. The different lattice direction and typical amorphous diffraction pattern (Fig. 3f) suggest that the $NiCo_2O_4$@$NiCo_2O_4$ nanostructure is a mixture of crystal and amorphous phases, indicating poor crystalline in good agreement with the XRD results.

The XRD patterns of the obtained ACT, $NiCo_2O_4$ nanowire/ACT, and $NiCo_2O_4$@$NiCo_2O_4$/ACT are respectively shown in Fig. 4b. The peak at about 21° was identified to be the amorphous carbon from ACTs. The diffraction peaks in the XRD patterns of $NiCo_2O_4$/ACT and $NiCo_2O_4$@$NiCo_2O_4$/ACT can be indexed to the (111), (220), (311), (511) and (440) planes of the cubic $NiCo_2O_4$ phase (JCPDS card no. 20-0781).[41] No foreign peaks were detected, indicating that both of the core and shell are pure $NiCo_2O_4$. The diffraction peak of ACT at 21° is hidden in the relative intense diffraction peak (111) of $NiCo_2O_4$ at 19° of the XRD patterns of the $NiCo_2O_4$/ACT and $NiCo_2O_4$@$NiCo_2O_4$/ACT. The relatively weaker intensity of the $NiCo_2O_4$ peaks in the hybrid $NiCo_2O_4$/ACT and $NiCo_2O_4$@$NiCo_2O_4$/ACT indicates low crystallinity, which is beneficial for the improvement of specific capacitance.[42] XPS measurements were performed to explore the chemical states and compositions of the as-prepared $NiCo_2O_4$@$NiCo_2O_4$/ACT hybrid (Figs. 4c and d). The cobalt 2p XPS spectra consist of two spin-orbit doublets at 781.9 eV and 797.8 eV, respectively, pointing towards Co^{2+} and Co^{3+}, and two shakeup satellites at

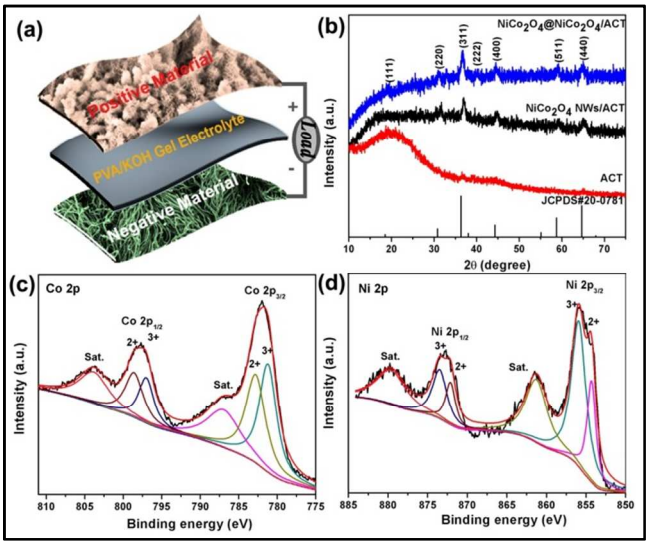

Fig. 4 (a) Illustration of the assembled flexible all-solid-state asymmetric supercapacitor; (b) XRD patterns of the as-obtained ACT, $NiCo_2O_4$ nanowire/ACT, and $NiCo_2O_4$@ $NiCo_2O_4$/ACT; (c) Co 2p and and (d) Ni 2p XPS spectra of $NiCo_2O_4$@$NiCo_2O_4$/ACT.

786.9 eV and 803.8 eV (identified as "Sat.") (Fig. 4c). Similarly, the nickel 2p XPS spectra consist of two spin-orbit doublets at 872.8 eV and 855.7 eV, resulting from Ni^{2+} and Ni^{3+}, and two shakeup satellite peaks at 879.8 and 861.3 eV (Fig. 4d).[43,44]

3.2 Electrochemical Performance

The CV curves of the ACT and $NiCo_2O_4$ nanowire/ACT hybrid at the scan rates of 5, 10, 25, 50, 75, 100 mV/s with the potential windows ranging from -0.2 to 0.5 V versus SCE in 6 M KOH aqueous solution can be found in Figs. S2a and c in the Supporting Information**.** The quasi-rectangular shape of CV curves for ACT (Fig. S2a) indicates ideal electrical double layer capacitive behavior. The CV curve of the $NiCo_2O_4$/ACT hybrid shows a more complicated shape with two pairs of redox peaks, which correspond to Faradaic redox reactions of $NiCo_2O_4$ that can be expressed in the following equations.[45]

$$NiCo_2O_4 + OH^- + H_2O \longleftrightarrow NiOOH + 2CoOOH + 2e^-$$

$$CoOOH + OH^- \longleftrightarrow CoO_2 + H_2O + e^-$$

The calculated specific capacitances from the CV curves can be found in Fig. S2b and d in the Supporting Information. The specific capacitances of ACT electrode are 120, 85, 49.4, 33.1, 26.3, 22.3 F/g at the scan rates of 5, 10, 25, 50, 75, 100 mV/s, respectively, while the specific capacitances of the $NiCo_2O_4$ nanowire/ACT are respectively 1679, 902, 550, 348, 301 F/g (based on the mass of $NiCo_2O_4$) at the scan rates of 10, 25, 50, 75, 100 mV/s. The remarkably improved capacitance of the $NiCo_2O_4$/ACT results from the high pesudocapacitance of $NiCo_2O_4$ nanowires.[46] The decay of specific capacitance with increasing scan rate is due to the slow current accumulating process at low scan rates, which enables full access of active pores/sites, corresponding to its pseudocapactive feature. Overall, the ACT electrode shows better rate performance while the $NiCo_2O_4$ nanowires possess high specific capacitance. The coupling of the ACT and $NiCo_2O_4$ nanowires renders the $NiCo_2O_4$ nanowire/ACT electrode higher electrochemical performance.

Fig. S3a shows the CV curves obtained from the $NiCo_2O_4$@$NiCo_2O_4$/ACT electrode in 6 M KOH aqueous solution within the potential range of -0.2-0.5 V (vs SCE) at different scan rates. Two pairs of peaks were found in each individual CV curve, indicating that the capacitance is mainly based on the Faradaic redox reaction. The well-retained shape of CV curve with an increase in scan rate suggests that the porous nanostructure of $NiCo_2O_4$@$NiCo_2O_4$/ACT hybrid electrode is indeed beneficial to the fast redox reaction. Furthermore, it is evident that each curve at different scan rates keeps similar redox couples, indicating the quasi-reversible and continuous faradic redox during the charge/discharge processes. The galvanostatic charge/discharge curve (Fig. S3b) of the $NiCo_2O_4$@$NiCo_2O_4$/ACT electrode at a low current density (1 mA/cm^2) exhibits two voltage stages which result from the pseudocapacitive feature of the electrode, agreeing well with the aforementioned CV study. The specific capacitances of the $NiCo_2O_4$@$NiCo_2O_4$/ACT hybrid electrode were calculated to be 1929, 1764, 1367, 1046, 771 and 576 F/g from the discharge curves at the current densities of 1, 2.5, 5, 10, 15 and 20 mA/cm^2, respectively (Fig. S3c). The well-defined hierarchical $NiCo_2O_4$@$NiCo_2O_4$ core/shell nanostructure increases the exposed active surface area for electrolyte and provides an express-path for the diffusion of electrolyte ions, leading to the high mass specific capacitance. The small equivalent series resistance (ESR) (0.27 Ω) and charge-transfer resistance (R_{ct}) (3.61 Ω) obtained from the Nyquist plots of electrochemical impedance spectra (EIS) (calculated by the method given in Ref 44)[47] of the $NiCo_2O_4$@$NiCo_2O_4$/ACT electrode are supportive of the remarkable electrochemical performance.

The CV curves and Nyquist plots of the ACT, $NiCo_2O_4$ nanowire/ACT and $NiCo_2O_4$@$NiCo_2O_4$/ACT electrodes are comparatively shown in Fig. S4 in the Supporting Information. The CV curve of the ACT shows electrical double layer characteristics with a rectangular shape, while the CV curves of the $NiCo_2O_4$ nanowire/ACT and $NiCo_2O_4$@$NiCo_2O_4$/ACT

electrodes exhibit typical pseudocapacitive features with two pairs of redox peaks (Fig. S4a in the Supporting Information). Compared with the ACT and $NiCo_2O_4$ nanowire/ACT electrodes, the larger integrated area of the current-potential curves (Fig. S4a) and reduced charge-transfer resistance (Fig. S4b) of the $NiCo_2O_4$@$NiCo_2O_4$/ACT hybrid electrode indicate improved electrochemical performance, which is attributed to the intriguing hierarchical core/shell architecture with a plethora of internal mesopores, facilitating both mass and ions transport during the charging/discharging process. Long lifespan is a key factor for evaluating the practical application of supercapacitor electrode. Fig. S5 shows the cyclic performance of the $NiCo_2O_4$@$NiCo_2O_4$/ACT hybrid electrode conducted by the galvanostatic charge/discharge tests at a current density of 20 mA/cm^2 for up to 1000 cycles. The $NiCo_2O_4$@$NiCo_2O_4$/ACT hybrid electrode exhibits a high specific capacitance and eminent cyclic stability with an increase of capacitance for the initial 50 cycles and 3.98 % increase after 1000 cycle tests, which are ascribed to the full exposure of active Ni and Co sites to the electrolyte after the repetitive charge/discharge. The results obtained from the three electrode test system jointly show that the $NiCo_2O_4$@$NiCo_2O_4$/ACT is an exceptional supercapacitor electrode material in terms of high specific capacitance, excellent rate performance, long lifespan and low charge transfer resistance.

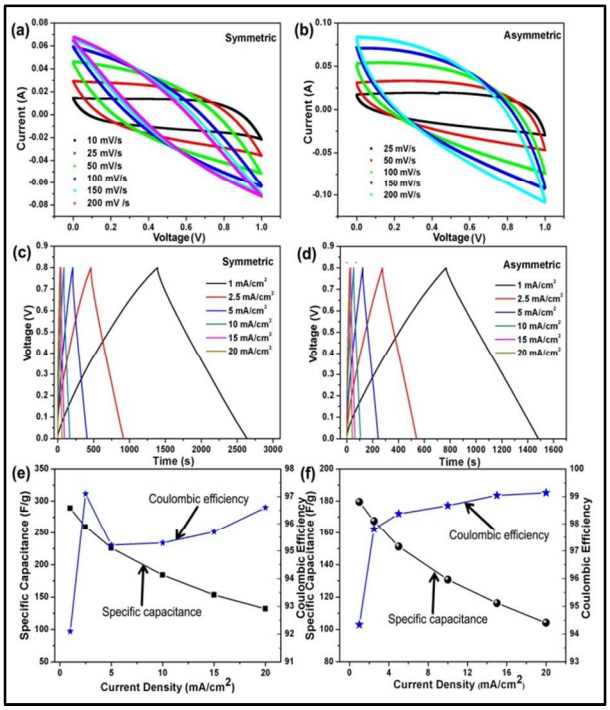

Fig. 5 (a) CV curves of the symmetric supercapacitor with $NiCo_2O_4$@$NiCo_2O_4$/ACT as both the positive electrode and negative electrode, PVA/KOH as polymer gel electrolyte; (b) CV curves of the asymmetric supercapacitor with $NiCo_2O_4$@$NiCo_2O_4$/ACT hybrid as the positive electrode, ACT as the negative electrode, and PVA/KOH as polymer gel electrolyte, respectively; (c) Charge/discharge curves of the symmetric supercapacitor with $NiCo_2O_4$@$NiCo_2O_4$/ACT as both the positive electrode and negative electrode, PVA/KOH as polymer gel electrolyte; (d) Charge/discharge curves of the asymmetric supercapacitor with $NiCo_2O_4$@$NiCo_2O_4$/ACT hybrid as the positive electrode, ACT as the negative electrode, and PVA/KOH as polymer gel electrolyte, respectively; (e) Specific capacitances and coulombic efficiency of the symmetric supercapacitor with $NiCo_2O_4$@$NiCo_2O_4$/ACT as both the positive electrode and negative electrode, PVA/KOH as polymer gel electrolyte at different current densities; (f) Specific capacitances and coulombic efficiency of the asymmetric supercapacitor with $NiCo_2O_4$@$NiCo_2O_4$/ACT hybrid as the positive electrode, ACT as the negative electrode, and PVA/KOH as polymer gel electrolyte, respectively.

However, the three-electrode configuration could not fully reflect the real electrochemical performance of an electrode in real-world applications, because only one electrode contains the test material and the applied voltage and charge transfer across the single electrode are markedly different from the two-electrode configuration.[48] To examine the practical performance of the $NiCo_2O_4$@$NiCo_2O_4$/ACT in a packaged cell, we assembled both symmetric and asymmetric flexible supercapacitors. Here ACT was chosen as the negative electrode to assemble a $NiCo_2O_4$@$NiCo_2O_4$/ACT//ACT asymmetric supercapacitor, as illustrated in the inset of Fig. 4a. The CV curves of the $NiCo_2O_4$@$NiCo_2O_4$/ACT symmetric and asymmetric supercapacitors were collected at different scan rates, as demonstrated in Fig. 5a and b. The CV curves of both symmetric and asymmetric supercapacitors exhibit nearly rectangular shape at slow scan rates, corresponding to the excellent synergistic effect of double-layer capacitive ACT and pseudocapactive $NiCo_2O_4$. However, with the scan rate increasing, the obvious deviation from rectangularity of the symmetric supercapacitor suggests higher charge transfer resistance and poor rate performance. The constant current charge/discharge curves of the symmetric and asymmetric at different current densities (1, 2.5, 5, 10, 15 and 20 mA/cm^2) are shown in Fig. 5c and d. The charge/discharge curves for both the symmetric and asymmetric supercapacitors are almost symmetric with a small internal resistance (IR) drop, indicating a good electrochemical capacitive characteristic and superior reversible redox reaction. Rate capability and coulombic efficiency are two important factors for evaluating the power applications of supercapacitors. The corresponding specific capacitances for the symmetric supercapacitor are 288 F/g at 1 mA/cm^2 and 131 F/g at 20 mA/cm^2, showing 45.48% of capacitance retention after the current density was increased 20 times (Fig. 5e). The specific capacitances for the asymmetric supercapacitor are 179 F/g at 1 mA /cm^2 and 104 F/g at 20 mA/cm^2, respectively, and 58.1% of the capacitance is retained (Fig. 5f), suggest better rate performance of the asymmetric supercapacitor, agreeing well with the CV results. Compared with the symmetric supercapacitor, the asymmetric supercapacitor exhibited relatively "poor" capacitance performance, probably due to the practical capacitance mismatch of positive and negative electrodes. The initial coulombic efficiency values of the symmetric and asymmetric cells were calculated to be 92.01% and 94.3% at 1 mA/cm^2, respectively. The coulombic efficiency of the symmetric cell quickly increased to the peak value of 97.16%, immediately followed by a decrease and then a slow increase with the increase of current density. For the asymmetric cell, the coulombic efficiency exhibited a fast increase at the initial stage and then a gradual increase up to 99.16%. The high coulombic efficiency helps enhance the energy utilization efficiency and promote electrochemical reversibility.

To further explore the potential of the asymmetric supercapacitor, the applied voltage was extended to 1.6 V (Fig. 6a). The asymmetric cell exhibited a stable potential window even at the high voltage window, which is essential for

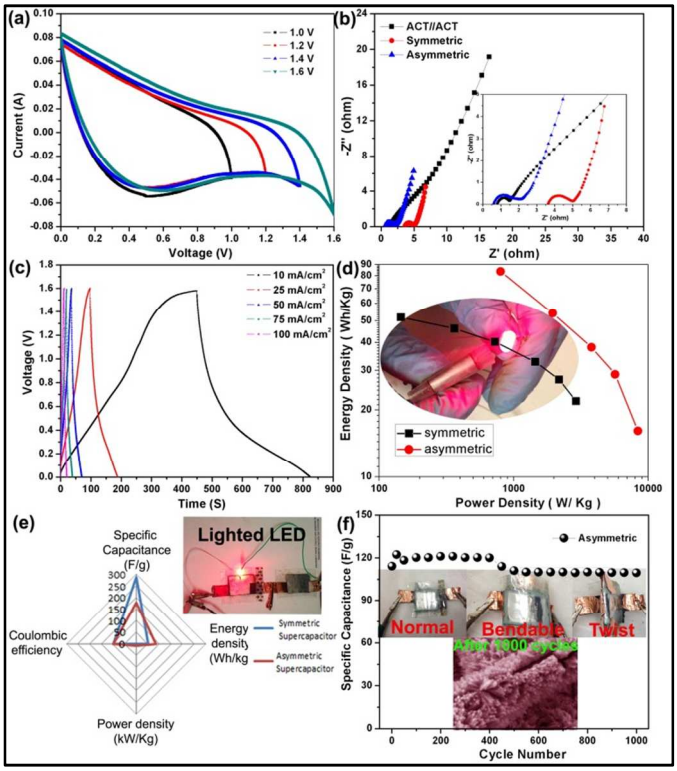

Fig. 6 (a) CV curves of $NiCo_2O_4$@$NiCo_2O_4$/ACT//ACT asymmetric supercapacitor with PVA/KOH polymer gel electrolyte under the voltage windows of 1, 1.2, 1.4 and 1.6 V at the scan rate of 50 mV/s; (b) Nyquist plots of the ACT//ACT symmetric supercapacitor with PVA/KOH polymer gel electrolyte, $NiCo_2O_4$@$NiCo_2O_4$/ACT//ACT asymmetric supercapacitor with PVA/KOH polymer gel electrolyte and $NiCo_2O_4$@$NiCo_2O_4$/ACT//$NiCo_2O_4$@$NiCo_2O_4$/ACT symmetric supercapacitor with PVA/KOH polymer gel electrolyte; (c) charging/discharging curves of asymmetric supercapacitor with PVA/KOH polymer gel electrolyte at different current densities; (d) Ragone plots of the as-assembled $NiCo_2O_4$@$NiCo_2O_4$/ACT//ACT asymmetric supercapacitor with PVA/KOH polymer gel electrolyte, and $NiCo_2O_4$@$NiCo_2O_4$/ACT//$NiCo_2O_4$@$NiCo_2O_4$/ACT symmetric supercapacitor with PVA/KOH polymer gel electrolyte (inset is a red light-emitting diode (LED) lighted by two asymmetric supercapacitors under folded state); (e) Radar plot of the symmetric supercapacitor and asymmetric supercapacitor, inset is a lighted LED by two asymmetric supercapacitors connected in series; (f) Cycling performance of $NiCo_2O_4$@$NiCo_2O_4$//ACT asymmetric supercapacitor with PVA/KOH polymer gel electrolyte under normal, bent and twisted state at a current density of 15 mA/cm^2 (inset is the SEM image of $NiCo_2O_4$@$NiCo_2O_4$/ACT obtained after 1000 cycles).

practical applications. Fig. 6c shows the GV curves of the asymmetric supercapacitor at different current densities. The asymmetric cell exhibited a high capacitance retention 60 F/g At the current density 100 mA/cm^2, indicating excellent rate performance. The EIS tests were carried out for an in-depth understanding of the electrochemical behavior of the assembled symmetric and asymmetric flexible cells. The Nyquist plots of the ACT//ACT cell, $NiCo_2O_4$@$NiCo_2O_4$/ACT//$NiCo_2O_4$@$NiCo_2O_4$/ACT symmetric cell and $NiCo_2O_4$@$NiCo_2O_4$/ACT//ACT asymmetric cell are compared in Fig. 6b. In the high frequency range, the intercept of the semicircle with the real axis represents the equivalent series resistance (ESR), which includes the ionic resistance, the intrinsic resistance, and the contact resistance at the electrode/current collector interface.[49] Clearly, the smaller ESR of the $NiCo_2O_4$@$NiCo_2O_4$/ACT//ACT asymmetric cell results from the hierarchical porous nanostructure of the $NiCo_2O_4$@$NiCo_2O_4$/ACT electrode, which facilitates the access of electrolyte ions to the active surface and shortens the ion diffusion path. A straight line close to 90° was found for the asymmetric cell in the low frequency range, indicating a pure capacitive behavior and low diffusion resistance of electrolyte ions in the core of the electrode.[50]

Energy density and power density are crucial factors for evaluating the practical application of supercapacitors. A good supercapacitor is expected to provide both high energy density and high capacitance at high charge/discharge rates. The Ragone plots of the all-solid-state flexible $NiCo_2O_4$@$NiCo_2O_4$/ACT//$NiCo_2O_4$@$NiCo_2O_4$/ACT symmetric cell and $NiCo_2O_4$@$NiCo_2O_4$/ACT//ACT asymmetric cell are shown in Fig. 6d. As the plots show, the values and trends of energy and power densities for both symmetric and asymmetric cells are similar. For the symmetric cell, the energy density decreases from 51.6 down to 23.3 Wh/kg, while the power density increases from 144 up to 2943 W/kg. Compared with symmetric cell, the asymmetric cell shows higher energy density of 83.6 Wh/kg at a high power density of 800 W/kg, and remains 21.16 Wh/Kg at the power density of 8.4 kW/kg. Clearly, the asymmetric supercapacitor exhibits much higher power density than that of the symmetric cell. The comprehensive performances for both symmetric and asymmetric cells were compared in the radar plots in Fig. 6e, indicating the synergistic effects of ACT and hierarchical $NiCo_2O_4$ nanostructure.

A long cycling lifespan is another important requirement for supercapacitor applications. The cycle stability of $NiCo_2O_4$@$NiCo_2O_4$/ACT//ACT asymmetric cell was evaluated by repeating the constant current charge/discharge test under different states (normal, bent and twisted states) at a current density of 15 mA/cm^2 for 1000 cycles (Fig. 6f). The asymmetric cell showed an increase in specific capacitance at the initial normal state, which is ascribed to the incomplete exposure of Ni and Co active sites to the gel electrolyte. There is almost no specific capacitance loss after 1000 charge-discharge even at the bent and twisted states, indicating excellent robustness and flexibility. The insets of Fig. 6d and Fig. 6f show the digital photographs of the as-assembled flexible supercapacitor packed with PET tape. To demonstrate its practical application, two pieces of the as-assembled flexible all-solid-state cells in series were used to light a commercial red LED (inset of Fig. 6e). Even in hash conditions such as folded state (inset of Fig. 6d), the brightness of the lightened LED did not change, showing its robust functionality and excellent flexibility. The inset of Fig. 6f is the SEM image of the $NiCo_2O_4$@$NiCo_2O_4$/ACT electrode after 1000 cycles (without dipping polymer electrolyte during the test). It can be seen that the morphology of the $NiCo_2O_4$@$NiCo_2O_4$ core/shell

architecture well remained in the entire charge/discharge process, ensuring the excellent electrochemical performance of the flexible electrode.

In real-world applications, flexible supercapacitors should be able to provide power under harsh environments, such as wearable, bendable, stretchable or twisted states, requiring that both the current collector and electrode have both flexibility and stability. To enhance the mechanical robustness of a supercapacitor without sacrificing its flexibility, a 200 μm thick transparent solid-state polymer electrolyte film was fabricated to severe as both separator and electrolyte. Furthermore, the $NiCo_2O_4$@$NiCo_2O_4$/ACT hybrid electrode was coated with polymer electrolyte to further improve its mechanical performance. Fig. 7a shows the digital photograph of such prepared solid state electrolyte film and polymer gel electrolyte. After dipped in the polymer electrolyte, the interspace of the $NiCo_2O_4$@$NiCo_2O_4$ core/shell was filled with gel electrolyte (Figs. 7b and c), which not only improves the accessibility of electrolyte ions but also intensifies the mechanical strength of the flexible electrode. Fig. 7 d shows the tensile stress-strain curves of the pure ACT and $NiCo_2O_4$@$NiCo_2O_4$/ACT hybrid electrode dipped with the polymer gel electrolyte. Compared with the pure ACT, the tensile strength of the $NiCo_2O_4$@$NiCo_2O_4$/ACT electrode dipped with polymer gel electrolyte increases to 0.97 MPa, which is 6.5 times higher than that of pure ACT (0.15 MPa).

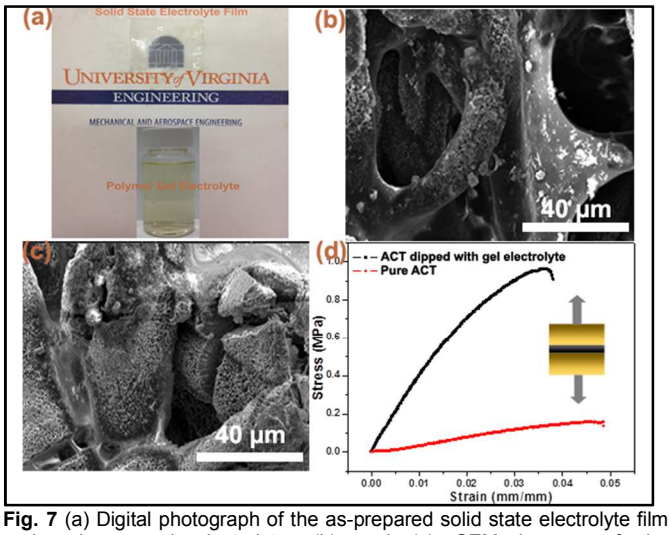

Fig. 7 (a) Digital photograph of the as-prepared solid state electrolyte film and polymer gel electrolyte; (b) and (c) SEM images of the $NiCo_2O_4$@$NiCo_2O_4$/ACT dipped with the polymer gel electrolyte; (d) Tensile stress-strain curves of the $NiCo_2O_4$@$NiCo_2O_4$/ACT dipped with the polymer gel electrolyte and pure ACT, respectively.

Clearly, the design of the hierarchical $NiCo_2O_4$@$NiCo_2O_4$/ACT core/shell nanostructure with the mesoporous $NiCo_2O_4$ nanowires as "core" and upright grown flaky $NiCo_2O_4$ nano-sheets as "shell" on high conductive ACTs advances the development of flexible textile supercapacitors. The high electrochemical performance of the $NiCo_2O_4$@$NiCo_2O_4$/ACT hybrid electrode is attributed to the following unique features of the design. First, the activated carbon fibers serve as highly conductive backbones, allowing for efficient current collection and rapid access of electrolyte ions to the surfaces of the active materials. Second, the mesoporous $NiCo_2O_4$ nanowires with high conductivity directly grew on the conductive substrates, reducing the contact resistance between electrode materials and charge collectors. Third, the ultrathin $NiCo_2O_4$ nanoflakes well wrapped around the $NiCo_2O_4$ nanowires to form a porous nanostructure, which shortens the electrolyte ion diffusion path, and enables faster kinetics and higher utilization of active material. More importantly, both core and shell are of the same material-$NiCo_2O_4$, eliminating the contact resistance of dissimilar materials. Finally, the polymer gel electrolyte fully penetrated into the interspace of the core/shell nanostructure, which not only highly increases accessibility of electrolytic ions, but also improves the mechanical property of the $NiCo_2O_4$@$NiCo_2O_4$/ACT hybrid, making it more suitable for practical applications.

4. Conclusions

We have synthesized hierarchical $NiCo_2O_4$@$NiCo_2O_4$ core/shell nanostructure on flexible, cotton activated carbon textiles (ACTs) for supercapacitor electrodes using coupled hydrothermal synthesis and chemical bath deposition process. The hierarchical $NiCo_2O_4$ nanowire/$NiCo_2O_4$ nanoflake core/shell facilitated the access of electrolyte ions to the active surface and shortened the ion diffusion path, concurrently enhancing charge efficiency and pushing up redox capacitance. On the other hand, the activation of cotton textiles into porous, highly conductive ACTs with high accessible surface area endowed the asymmetric flexible supercapacitor with high rate performance. After dipped the flexible hybrid electrode with PVA-KOH solid-state gel which served as both the electrolyte and separator, the assembled $NiCo_2O_4$@$NiCo_2O_4$/ACT//ACT asymmetric supercapacitor exhibited not only high electrochemical performance in terms of high specific capacitance, excellent cycling stability, remarkable energy density and power density, but also an exceptional mechanical robustness. The coupling of outstanding electrochemical performance, superior flexibility, and excellent mechanical performance, promises that such solid-state textile based supercapacitors should boost the practical application of the flexible power source in the future portable/wearable electronics.

Acknowledgements

Financial support for this study was provided by the U.S. National Science Foundation (CMMI-1418696 and CMMI-1358673) and the i6 Virginia Innovation Partnership. The authors thank the staff members at the University of Virginia NMCF for electron microscopy technical support.

Notes and references

[a] Department of Mechanical and Aerospace Engineering
University of Virginia
122 Engineer's Way, Charlottesville, VA 22904-4746 (USA)
* Prof. X.D. Li, E-mail: xl3p@virginia.edu

1. J. M. Tarascon, *Phil. Trans. R. Soc. A,* 2010, ***368,*** 3227.
2. A. Burke, *J. Power Sources,* 2000, ***91,*** 37.
3. B. E. Conway, *Electrochemical Supercapacitors: Scientific Fundamentals and Technological Applications,* Kluwer Academic Publishers/Plenum Press, New York, **1999**.
4. X. H. Lu, M. H. Yu, G. M. Wang, Y. X. Tong and Y. Li, *Energy Environ. Sci.,* 2014, ***7,*** 2160
5. A. E. Fischer, K. A. Pettigrew, D. R. Rolison, R. M. Stroud and J. W. Long, *Nano Lett.,* 2007, ***7,*** 281.

6. K. Fic , G. Lota , M. Meller and E. Frackowiak, *Energy Environ. Sci.,* 2012, ***5,*** 5842.
7. M. Deschamps, E. Gilbert, P. Azais, E. Raymundo-Piñero, M. R. Ammar, P. Simon, D. Massiot and F. Béguin, *Nat. Mater.,* 2013, ***12,*** 351.
8. V. Ruiz, T. Huynh, S. R. Sivakkumara and A. G. Pandolfo, *RSC Adv.,* 2012, ***2,*** 5591.
9. M. Koo, K. Park, S. H. Lee, M. Suh, D. Y. Jeon, J. W. Choi, K. Kang and K.. J. Lee, *Nano Lett.,* 2012, ***12,*** 4810.
10. H. Pan, J. Li and Y. P. Feng, *Nanoscale Res Lett.* 2010, **5,** 654.
11. G. H. Yu, L. B. Hu, M. Vosgueritchian, H. L. Wang, X. Xie, J. R. McDonough, X. Cui, Y. Cui and Z. N. Bao, *Nano Lett.* 2011, ***11,*** 2905.
12. L. B. Hu, M. Pasta, F. La Mantia, L. F. Cui, S. Jeong, H. D. Deshazer, J. W. Choi, S. M. Han and Y. Cui, *Nano Lett.* 2010, ***10,*** 708.
13. G. Zhang and X. W. Lou, *Sci. Rep.* 2013, ***3,*** 170.
14. H. Wang and X. Wang, *ACS Appl. Mater. Interfaces,* 2013, ***5,*** 6255.
15. K. Jost, G. Dion and Y. Gogotsi, *J. Mater. Chem. A,* 2014, ***2,*** 10776.
16. L. H. Bao and X. D. Li, *Adv. Mater.,* 2012, ***24,*** 3246.
17. G. Yu, L. Hu, N. Liu, H. Wang, M. Vosgueritchian, Y. Yang, Y. Cui, and Z. N. Bao, *Nano Lett.,* 2011, ***11,*** 4438.
18. G. Xiong, K. Hembram, R. G. Reifenberger, and T. S. Fisher, *J. Power Sources,* 2013, ***227,*** 254.
19. L. Shen, Q. Che, H. Li and X. Zhang, *Adv. Funct. Mater.,* 2014, ***24,*** 2630.
20. W.W. Zhou, J. Liu, T. Chen, K. S. Tan, X. Jia, Z. Luo, C. Cong, H. Yang, C. M. Li and T. Yu, *Phys. Chem. Chem. Phys.*, 2011, ***13,*** 14462.
21. C. Yuan, X. Zhang, L. Su, B. Gao and L. Shen, *J. Mater. Chem.,* 2009, ***19,*** 5772.
22. Z. Gao, J. Wang, Z. Li, W. Yang, B. Wang, M. Hou, Y. He, Q. Liu, T. Mann, P. Yang, M. Zhang, and L. Liu, Chem. Mater. 2011, **23,** 3509.
23. C. Meng, C. Liu, L. Chen, C. Hu, and S. Fan, *Nano Lett.,* 2010, ***10,*** 4025.
24. G. Xiong, C. Meng, R. G. Reifenberger, P. P. Irazoqui and T. S. Fisher, *Adv. Energy Mater.2014,* ***4,*** 1300515.
25. Z. Lu, Q. Yang, W. Zhu, Z. Chang, J. Liu, X. Sun, D. Evans and X. Duan, *Nano Research,* 2012, ***5,*** 369.
26. Z. Chen, V. Augustyn, J. Wen, Y. Zhang, M. Shen, B. Dunn and Y. Lu, *Adv. Mater.,* 2011, ***23,*** 791.
27. H. Jiang, J. Ma and C. Z. Li, *Chem. Commun.,* 2012, ***48,*** 4465.
28. L. Huang, D. Chen, Y. Ding, S. Feng, Z. L. Wang and M. L. Liu, *Nano Lett.,* 2013, ***13,*** 3135.
29. Y. Dai, S. Tang, S. Vongehr, and X, Meng, *ACS Sustainable Chem. Eng.,* 2014, ***2,*** 692.
30. G. Zhang, T. Wang, X. Yu, H. Zhang, H. Duan and B. Lu, *Nano Energy*, 2013, ***2,*** 586.
31. D. P Cai, B. Liu, D. D Wang, L. L. Wang, Y. Liu, H. Li, Y. R. Wang, Q. H. Lia and T. H. Wang, *J. Mater. Chem. A,* 2014, ***2,*** 4954.
32. L. Yu, G. Zhang, C. Yuan and X. W. Lou, *Chem. Commun.,* 2013, ***49,*** 137.
33. L. H. Bao, J. Zang and X. D. Li, *Nano Lett.,* 2011, ***11,*** 1215.
34. W. Yang, Z. Gao, J. Ma, X. Zhang, J. Wang and J. Liu, *J. Mater. Chem. A,* 2014, ***2,*** 1448.
35. C. Yilmaz, A. E. Cetin, G. Goutzamanidis, J. Huang, S. Somu, H. Altug, D. Wei, and A. Busnaina, *ACS Nano,* 2014, ***8,*** 4547.
36. Q. Wang, X. Wang, B. Liu, Gang Yu, X. Hou, D. Chen and G. Shen, *J. Mater. Chem. A*, 2013, ***1,*** 2468.
37. J. Du, G. Zhou, H. Zhang, C. Cheng, J. Ma, W. Wei, L. Chen and T. Wang, *ACS Appl. Mater. Interfaces*, 2013, ***5,*** 7405.
38. X. Y. Yu, X. Z. Yao, T. Luo, Y. Jia, J. H. Liu and X. J. Huang, *ACS Appl. Mater. Interfaces*, 2014, ***6,*** 3689.
39. X. Liu, S. Shi, Q. Xiong, L. Li, Y. Zhang, H. Tang, C. Gu, X. Wang and J. Tu, *ACS Appl. Mater. Interfaces*, 2013, ***5,*** 8790.
40. M. R. Tarasevich and B. N. Efremov, Electrodes of Conductive Metallic Oxides, Part A, Elsevier, USA, **1982**, 227.
41. S. Verma, H. M. Joshi and T. Jagadale, *J. Phys. Chem. C,* 2008, ***112,*** 15106.
42. R. R. Salunkhe, K. Jang, H. Yu, S. Yu, T. Ganesh, S. H. Han and H. Ahn, *J. Alloys Compd.* 2011, ***509,*** 6677.
43. R. Ding, L. Qi, M. J. Ji and H. Y. Wang, *Nanoscale,* 2014, ***6,*** 1369.
44. J. G. Kim, D. L. Pugmire, D. Battaglia and M. A. Langell, *Appl. Surf. Sci.,* 2000, ***165,*** 70.
45. C. C. Hu and C. Y. Cheng, *Electrochem. Solid-State Lett.* 2002, ***5,*** A43.
46. T. Y. Wei, C. H. Chen, H. C. Chien, S. Y. Lu and C. C. Hu, *Adv. Mater.,* 2010, ***22,*** 347.
47. J. Wang, Z. Gao, Z. Li, B. Wang, Y. Yan, Q. Liu, T. Mann, M. Zhang and Z. Jiang, *J. Solid State Chem.* 2011, ***184,*** 1421.
48. M. D. Stoller and R. S. Ruoff, *Energy Environ. Sci.,* 2010, ***3,*** 1294.
49. Z. Gao, W. Yang, J. Wang, B. Wang, Z. Li, Q. Liu, M. Zhang, and L. Liu, *Energy Fuels,* 2013, ***27,*** 568.
50. G. J. Brug, A. V. Eeden, M. Sluyters-Rehbach and J. H. Sluyters *J. Electroanal. Chem.,* 1984, ***176,*** 275.